

The limited growth of vegetated shear layers

M. Ghisalberti and H. M. Nepf

Ralph M. Parsons Laboratory, Department of Civil and Environmental Engineering, Massachusetts Institute of Technology, Cambridge, Massachusetts, USA

Received 17 October 2003; revised 18 February 2004; accepted 23 April 2004; published 7 July 2004.

[1] In contrast to free shear layers, which grow continuously downstream, shear layers generated by submerged vegetation grow only to a finite thickness. Because these shear layers are characterized by coherent vortex structures and rapid vertical mixing, their thickness controls exchange between the vegetation and the overlying water. Experiments conducted in a laboratory flume show that the growth of these obstructed shear layers is arrested once the production of shear-layer-scale turbulent kinetic energy (SKE) is balanced by dissipation of SKE within the canopy. This equilibrium condition, along with a mixing length closure scheme, was used in a one-dimensional numerical model to predict the mean velocity profiles of the experimental shear layers. The agreement between model and experiment is very good, but field application of the model is limited by a lack of description of the drag coefficient in a submerged canopy. *INDEX TERMS:* 1890 Hydrology: Wetlands; 4568 Oceanography: Physical: Turbulence, diffusion, and mixing processes; 4211 Oceanography: General: Benthic boundary layers; *KEYWORDS:* mixing length, shear layer, turbulence, vegetated flow, vortex

Citation: Ghisalberti, M., and H. M. Nepf (2004), The limited growth of vegetated shear layers, *Water Resour. Res.*, 40, W07502, doi:10.1029/2003WR002776.

1. Introduction

[2] Aquatic macrophyte communities, which include the plants as well as the plankton, benthic flora, and epiphytic organisms that live among them, depend on a supply of nutrients from the surrounding water column [e.g., *Short et al.*, 1990; *Taylor et al.*, 1995]. In turn, these communities play an important role in maintaining the water quality of coastal regions by filtering nutrients from the water column [*Short and Short*, 1984]. Submerged macrophytes also provide an important habitat for invertebrate larvae [e.g., *Phillips and Menez*, 1988]. Settlement and recruitment of larvae to this habitat depend not only on organism behavior but also on hydrodynamic processes at many scales in and around the canopy (as reviewed by *Butman* [1987], also by *Eckman* [1983], *Duggins et al.* [1990], *Gambi et al.* [1990], and *Grizzle et al.* [1996]). The drag exerted by the vegetation promotes sediment accumulation by reducing the near-bed stress [*Lopez and Garcia*, 1997], and this is also expected to strongly influence the vertical transport of chemicals released by the sediment. This paper presents predictive models for key aspects of the canopy-scale hydrodynamics, described below.

[3] The dominant hydrodynamic feature of flow with submerged macrophytes is a region of strong shear at the top of the canopy, created by the vertical discontinuity of the drag [*Gambi et al.*, 1990; *Nepf and Vivoni*, 2000]. Figure 1 shows the vertical profile of mean velocity for a flow with submerged, flexible vegetation (data taken from *Ghisalberti and Nepf* [2002]). The shear layer contains an inflection point, making it dynamically analogous to a mixing layer, with vertical transport through the layer dominated by

coherent, shear-scale, Kelvin-Helmholtz (KH) vortices [*Raupach et al.*, 1996; *Ikeda and Kanazawa*, 1996; *Ghisalberti and Nepf*, 2002]. These vortices therefore control the exchange of nutrients, larvae, and sediment between a submerged canopy and the overlying water. In an unobstructed mixing layer, the vortices grow continually downstream [e.g., *Brown and Roshko*, 1974]. In a vegetated mixing layer, however, the vortices grow to a finite size a short distance from their initiation [*Ghisalberti and Nepf*, 2002]. In many instances (as in Figure 1), the final vortex size, and the region of rapid exchange it defines, extends to neither the water surface nor the bed. This segregates the canopy into an upper region of rapid exchange and a lower region with more limited water renewal [*Nepf and Vivoni*, 2000].

[4] The goal of this paper is to explain the dynamic equilibrium that arrests the growth of vortices formed in a vegetated shear layer. Once established, this equilibrium condition can be used, with simple turbulence closure, to predict the vertical velocity profile within and above submerged canopies. Previous studies have shown that the velocity profile above a vegetated boundary follows a logarithmic form, with velocity scale u_* defined by the turbulent stress at the top of the canopy and roughness scale z_o defined by canopy morphology [e.g., *Thom*, 1971; *Shi et al.*, 1995; *Nepf and Vivoni*, 2000]. However, the logarithmic form begins a full canopy height h above the actual top of the canopy (i.e., at $z = 2h$). The velocity profile within the canopy is often assumed to be uniform, resulting from a balance of vegetative drag and hydraulic gradient. The in-canopy and above-canopy profiles are then matched using semiempirical relations [e.g., *Kouwen et al.*, 1969; *Kouwen and Unny*, 1973]. Numerical models that use turbulence closure schemes in which the canopy elements are both a sink of mean flow energy and a source of turbulent energy

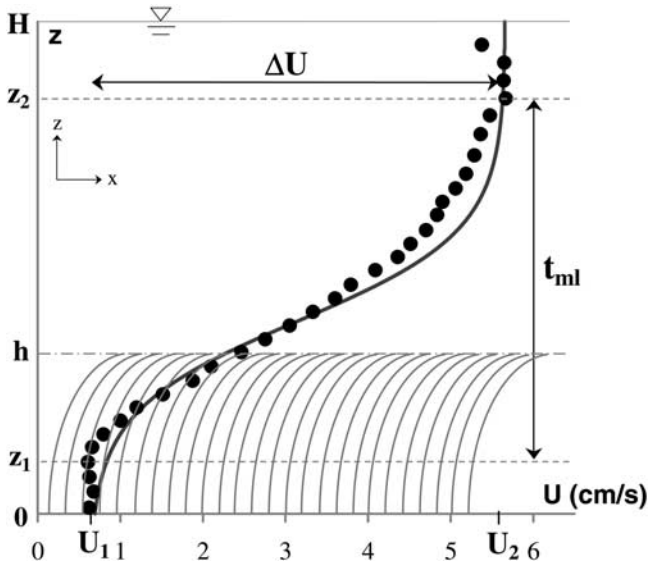


Figure 1. Mean velocity profile of a flow with submerged, flexible vegetation of height h (data taken from *Ghisalberti and Nepf* [2002]). The shear layer is defined by the limits z_1 (where the mean velocity is U_1) and z_2 (U_2), and has a thickness t_{ml} . The total shear across the layer is $\Delta U (= U_2 - U_1)$. The velocity profile contains an inflection point near the top of the vegetation. Despite its asymmetry, the profile qualitatively resembles the hyperbolic tangent profile (solid line) of a mixing layer.

have also been employed to predict velocity profiles in vegetated flows [e.g., *Burke and Stolzenbach*, 1983; *Lopez and Garcia*, 2001; *Nearby*, 2003]. These models, however, do not predict the cessation of shear layer growth.

2. Shear Layer Hydrodynamics

[5] This paper presents a one-dimensional approximation to a three-dimensional flow. The fully developed mean flow is assumed to be steady, parallel, and uniform in x and y (with coordinate directions defined in Figure 1). Using the standard Reynolds decomposition (i.e., $u_i = U_i + u_i'$) and an over bar to denote temporal averaging, the streamwise momentum equation takes the form

$$gS = \frac{\partial \overline{u'w'}}{\partial z} + \frac{1}{2} C_D a U^2, \quad (1)$$

where a represents the frontal area of the vegetation per unit volume, C_D is the drag coefficient of the canopy, and S is the surface slope ($= -dH/dx$). We note that vegetated shear flow is horizontally inhomogeneous at several scales [see, e.g., *Finnigan*, 2000], but in this analysis the inhomogeneity is removed by spatial averaging. Specifically, all velocity statistics presented in this paper, including those in equation (1), represent averages over the horizontal plane of local temporal means. In equation (1) we assume that the canopy is sufficiently dense that bed drag is negligible in comparison with canopy drag and the “dispersive flux” (which arises from spatial averaging) is negligible in comparison with the turbulent flux [see, e.g., *Brunet et al.*, 1994].

[6] There are two dominant turbulence scales in the flow: the shear (KH vortex) scale and the wake scale. The turbulent kinetic energy budget can be separated into these two distinct eddy scales, such that the canopy acts as a sink of shear-scale turbulent energy but as a source of wake-scale turbulent energy. As the KH vortices dominate vertical transport and govern shear layer growth, only the budget for shear-scale turbulent kinetic energy (SKE) will be considered here. Following *Shaw and Seginer* [1985], the budget for SKE in a vegetated shear layer can be written as

$$\frac{D\overline{k_s}}{Dt} = \underbrace{-\overline{u'w'}}_{(I)} \frac{\partial U}{\partial z} - \underbrace{\frac{\partial \overline{w'k_s}}{\partial z}}_{(II)} - \underbrace{\frac{1}{\rho} \frac{\partial \overline{w'p'}}{\partial z}}_{(III)} - \underbrace{\tilde{W}}_{(IV)} - \underbrace{\varepsilon_s}_{(V)} \quad (2)$$

where ρ is the fluid density, p is the pressure, and k_s is the instantaneous SKE. The terms on the right-hand side of equation (2) are shear production (I), turbulent transport of SKE (II), pressure transport (III), dissipation by canopy drag (IV), and viscous dissipation of SKE (V). Similarly to *Finnigan* [2000],

$$\tilde{W} \approx \frac{1}{2} C_D a U (2\overline{u'^2} + \overline{v'^2}), \quad (3)$$

where here it is expected that because of cylinder geometry, the dissipation of horizontal turbulent motions by the canopy will be much more pronounced than that of vertical turbulent motions. We assume that there is no export of SKE outside the shear layer. This assumption is supported by velocity spectra, which exhibit a clear peak at the vortex frequency inside the shear layer [*Ghisalberti and Nepf*, 2002], but not outside. If the pressure transport term in equation (2) is assumed to be due predominantly to shear-scale pressure fields (as in the work by *Zhuang and Amiro* [1994]), then integration of equation (2) between the lower and upper limits of the shear layer (z_1 and z_2 , respectively, as shown in Figure 1) eliminates the transport terms. Furthermore, we expect that drag dissipation of the shear-scale structures will dominate viscous dissipation [see, e.g., *Wilson*, 1988]. Therefore, for a fully developed vegetated shear layer ($D\overline{k_s}/Dt = 0$),

$$\int_{z_1}^{z_2} -\overline{u'w'} \frac{\partial U}{\partial z} dz = \int_{z_1}^{z_2} \frac{1}{2} C_D a U (2\overline{u'^2} + \overline{v'^2}) dz, \quad (4)$$

where h is the canopy height. We postulate that the growth of vegetated shear layers ceases once SKE production is countered exactly by canopy drag dissipation within the shear layer, much as bottom friction impedes the growth of shallow, horizontal shear layers [see, e.g., *Chu and Barbarutsi*, 1988]. We prove this using experimental observations.

[7] The integral conservation of SKE described in equation (4) can be simplified with the assumption of an appropriate eddy viscosity, ν_T . As the length scale of vertical transport (i.e., the vortex scale) is not significantly smaller than the distance over which the curvature of the mean shear changes appreciably, a flux-gradient model is not strictly valid [*Corrsin*, 1974]. However, many turbulent transport

problems violate this condition yet are modeled successfully with an eddy viscosity. Therefore the assumption of an eddy viscosity was deemed reasonable, if not strictly fundamentally valid. The eddy viscosity can be regarded as the product of a vertical turbulent length scale (which will scale upon the thickness of the shear layer, t_{ml}) and a vertical turbulent velocity (which will scale upon the total shear, ΔU). Although the turbulent length scale is expected to be constant throughout the shear layer, the turbulent velocity is not; the vortices create much stronger vertical velocity fluctuations along their centerline than at their edges. Thus v_T will be maximized at the vortex center, in the middle of the shear layer. So we may define

$$v_T = \frac{-\overline{u'w'}}{\partial U/\partial z} = C_1 \Delta U t_{ml} f(z^*), \quad (5)$$

where C_1 is a constant and $z^* = ((z - z_1)/t_{ml})$ is the fractional distance above the shear layer bottom. The shape function $f(z^*)$ is expected to peak in the middle of the shear layer, at $z^* = 0.5$.

[8] Within shear layers created by model aquatic vegetation, the vertical profile of $-\overline{u'w'}/(2u'^2 + v'^2)$ is similar across a wide range of canopy conditions (data taken from *Dunn et al.* [1996], $ad = 0.002 - 0.016$). This ratio increases from zero at $z^* = 0$ to a maximum at the top of the canopy, $z^* = (h - z_1)/t_{ml}$ (as also shown by *Nepf and Vivoni* [2000] and by our own unpublished data). Note that the ratio $(h - z_1)/t_{ml}$ represents the fraction of the shear layer that lies within the canopy and will henceforth be denoted by α . If we assume that the vertical profile of $-\overline{u'w'}/(2u'^2 + v'^2)$ has the same form as $f(z^*)$ but peaks at $z^* = \alpha$ rather than $z^* = 0.5$, then within the canopy

$$-\frac{\overline{u'w'}}{2u'^2 + v'^2} = \frac{C_2 f(z^*)}{(\alpha/0.5)}, \quad (6)$$

where C_2 is a constant. With equations (5) and (6), equation (4) becomes

$$\int_0^1 \left(\frac{\partial U}{\partial z^*} \right)^2 f(z^*) dz^* = \frac{t_{ml} \alpha}{C_2} \int_{z_1}^h C_D a U \frac{\partial U}{\partial z} dz. \quad (7)$$

[9] Because unbounded vegetated shear layers have no externally imposed length scale, it is reasonable to assume an approximate self-similarity of velocity profiles (as is done for all free shear flows). Furthermore, we will assume that $f(z^*)$ has a single, universal form in vegetated shear layers. Under these two assumptions, the left-hand side of equation (7) will scale upon $(\Delta U)^2$. So if $(C_D a)$ is assumed to be constant through the canopy, then equation (7) becomes

$$(\Delta U)^2 \sim (h - z_1) C_D a (U_h^2 - U_1^2), \quad (8)$$

where U_h and U_1 are the mean velocities at the top of the canopy and at the bottom of the shear layer, respectively. Recall that the scaling relationship in equation (8) holds if the production and drag dissipation of SKE are equal. As we postulate that shear layer growth ceases once this

equality is satisfied, it is expected that the stability parameter

$$\Omega = \frac{1}{(h - z_1) C_D a} \left(\frac{(\Delta U)^2}{U_h^2 - U_1^2} \right) \quad (9)$$

will be a universal constant for fully developed vegetated shear flows. At the beginning of shear layer development, SKE production outweighs dissipation and Ω (a scaled ratio of production to dissipation) will be high. The resulting increase in SKE is manifest as vortex growth, and thus an increase in $(h - z_1)$, such that Ω will decrease along the canopy until reaching its equilibrium value. SKE production and dissipation will then be equal and shear layer growth will cease. The following experiments were conducted to confirm the universal constancy of Ω in fully developed vegetated shear layers.

3. Experimental Methods

[10] Laboratory experiments were conducted in a 24-m-long, glass-walled recirculating flume with a width (b) of 38 cm (Figure 2). A constant flow depth (H) of 46.7 cm was employed. Smooth inlet conditions were created using a dense array of emergent cylinders to dampen inlet turbulence and a flow straightener to eliminate swirl. Model canopies consisted of circular wooden cylinders ($d = 0.64$ cm) arranged randomly in holes drilled into 1.26-m-long Plexiglas boards. Five boards were used, creating a model meadow 6.3 m in length. The packing density a was varied between 0.025 and 0.08 cm^{-1} , as described in Table 1. The range of dimensionless plant densities ($ad = 0.016 - 0.051$) is representative of dense aquatic meadows [see, e.g., *Chandler et al.*, 1996]. The average height of the canopy (h) was 13.8 or 13.9 cm (Table 1), changing slightly as dowels were added.

[11] Velocity measurements (u, v, w) were taken simultaneously by three three-dimensional (3-D) acoustic Doppler velocimeters (ADV), separated laterally by 10 cm (Figure 2). Velocity statistics from the three probes were averaged to obtain the spatial mean, as discussed earlier. All probes were located within the central 30 cm of the flume, outside of the sidewall boundary layers [*Nepf and Vivoni*, 2000]. Vertical profiles consisting of 32 ten-minute velocity records were collected at a sampling frequency of 25 Hz. Because of the configuration of the ADV probes, the uppermost 7 cm of the flow could not be sampled. An 8-cm-long slice of dowels (equivalent to 1.6–2.8 times the intercylinder spacing, ΔS) was removed across the channel to allow probe access. As shown by *Ikeda and Kanazawa* [1996], the removal of canopy elements over a short length ($7\Delta S$ in their study) has little impact upon the measured velocity statistics. All velocity profiles were measured at $x = 6.0$ m. Fully developed flow (i.e., $\partial/\partial x = 0$) was established well before this sampling point; e.g., t_{ml} and ΔU changed by less than 1% between $x = 4.6$ m and $x = 6.0$ m in run G.

[12] Eleven flow scenarios with varying values of discharge, Q , and a were examined (Table 1). The hydraulic radius Reynolds number ($\text{Re}_{Rh} = Q/\{\nu(2H + b)\}$) varied between 1250 (transitional) and 11,800 (fully turbulent). However, as discussed by *Ghisalberti and Nepf* [2002], the nature of vegetated flows is likely to be much more

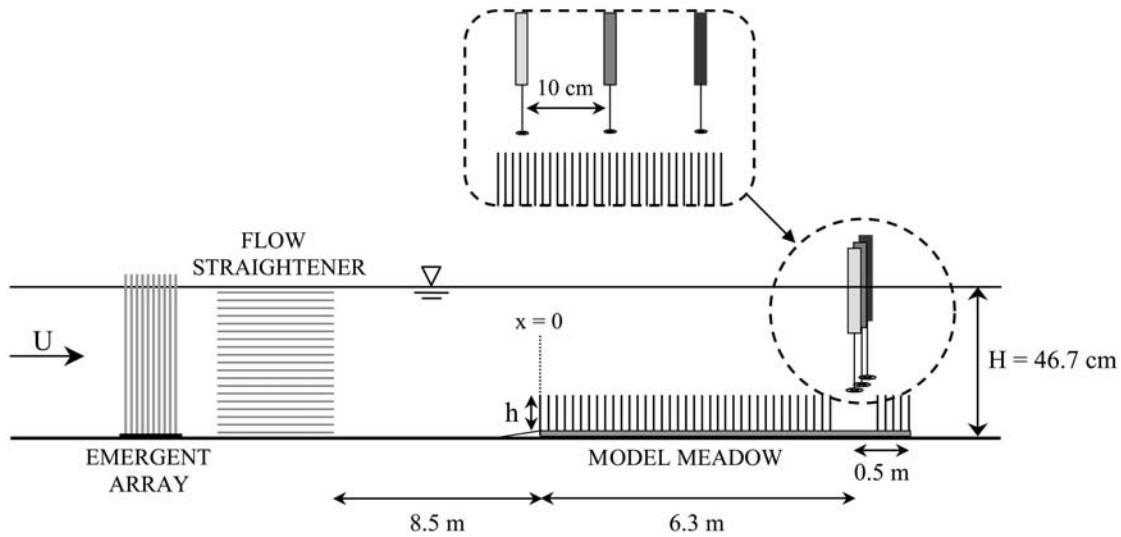


Figure 2. Side view of the 38-cm-wide laboratory flume (note the vertical exaggeration). Smooth inlet conditions were created using a dense array of emergent cylinders to dampen inlet turbulence and a flow straightener to eliminate swirl. Vertical profiles of 10-min velocity records were taken with three three-dimensional acoustic Doppler velocimeters at 25 Hz.

dependent upon the mixing layer Reynolds number ($Re_{ml} = \Delta U t_{ml} / \nu$). In unobstructed mixing layers, the transition from laminar to turbulent conditions is characterized by the development of small-scale turbulence superimposed upon the coherent vortical structures. This transition occurs over the range $Re_{ml} \approx 6 \times 10^3$ to 2×10^4 [Koochesfahani and Dimotakis, 1986]. As shown in Table 1, the flow scenarios of this study encompass values of Re_{ml} less than, within, and greater than the critical range.

[13] The surface slope S along the meadow was too small to be accurately measured by surface displacement gauges. Therefore S was estimated as

$$S = \frac{1}{g} \left[\frac{\partial \overline{u'w'}}{\partial z} \right], \quad h < z < z_2 \quad (10)$$

in accordance with equation (1). This method provided good estimates of the measured surface slope in the flume of

Dunn *et al.* [1996] and (in a previous study) the flume used here [Nepf and Vivoni, 2000]. As shown in Figure 3, the vertical profile of $u'w'$ within $h < z < z_2$ is clearly linear, allowing easy estimation of S . Above $z = z_2$, secondary circulation appears to significantly affect the vertical gradient of $u'w'$ [see Dunn *et al.*, 1996].

4. Experimental Results

4.1. Basic Properties of Velocity Profiles

[14] The parameters defining the vegetated shear layer in each experiment are listed in Table 1. In this table the cylinder Reynolds number has been evaluated using the velocity at the top of the canopy (i.e., $Re_d = U_h d / \nu$). The limits of the shear layer (i.e., z_1 and z_2) were taken as an average of the estimated locations of zero shear and of zero Reynolds stress.

[15] The vertical profiles of mean velocity and Reynolds stress for runs H and J ($a = 0.08 \text{ m}^{-1}$ for both) are shown in

Table 1. Summary of Experimental Conditions and Vegetated Shear Flow Parameters

	Run										
	A	B	C	D	E	F	G	H	I	J	K
$Q, \times 10^{-2} \text{ cm}^3 \text{ s}^{-1}$	48	17	74	48	143	94	48	143	94	48	17
$h, \text{ cm}$	13.9	13.9	13.9	13.9	13.8	13.8	13.8	13.8	13.8	13.8	13.8
$a, \text{ cm}^{-1}$	0.025	0.025	0.034	0.034	0.040	0.040	0.040	0.080	0.080	0.080	0.080
$S, \times 10^5$	0.99	0.18	2.5	1.2	7.5	3.2	1.3	10	3.4	1.3	0.26
$t_{mb} \pm 1.0 \text{ cm}$	32.8	25.3	31.4	30.7	35.4	33.5	28.8	33.9	32.7	28.5	21.8
$U_1, \text{ cm s}^{-1}$	1.3	0.50	1.7	1.1	3.5	2.4	1.1	2.7	1.7	0.77	0.27
$U_h, \text{ cm s}^{-1}$	2.5	1.0	3.5	2.4	6.7	4.6	2.3	6.3	4.0	2.1	0.93
$\Delta U, \text{ cm s}^{-1}$	3.2	1.3	4.9	3.5	9.5	6.0	3.3	11	7.4	3.9	1.7
$h - z_1, \pm 0.5 \text{ cm}$	12.5	9.0	11.7	11.3	11.3	10.9	10.5	10.6	9.6	8.3	6.4
α	0.38	0.36	0.37	0.37	0.32	0.32	0.36	0.31	0.29	0.29	0.29
$Re_{mb}, \times 10^{-4}$	1.1	0.32	1.6	1.1	3.7	2.2	1.0	3.8	2.4	1.1	0.36
Re_d	170	68	230	150	460	320	160	400	250	130	57
C_{Dh}	1.2	1.4	1.1	1.1	0.95	0.99	1.1	0.79	0.84	0.92	1.1

^aThe uncertainty of S , which was obtained through least squares regression, was estimated as roughly 5%. Likewise, U_1 , U_h , and ΔU represent lateral averages that approximate the horizontal mean with estimated uncertainties of 5%, 10%, and 2%, respectively.

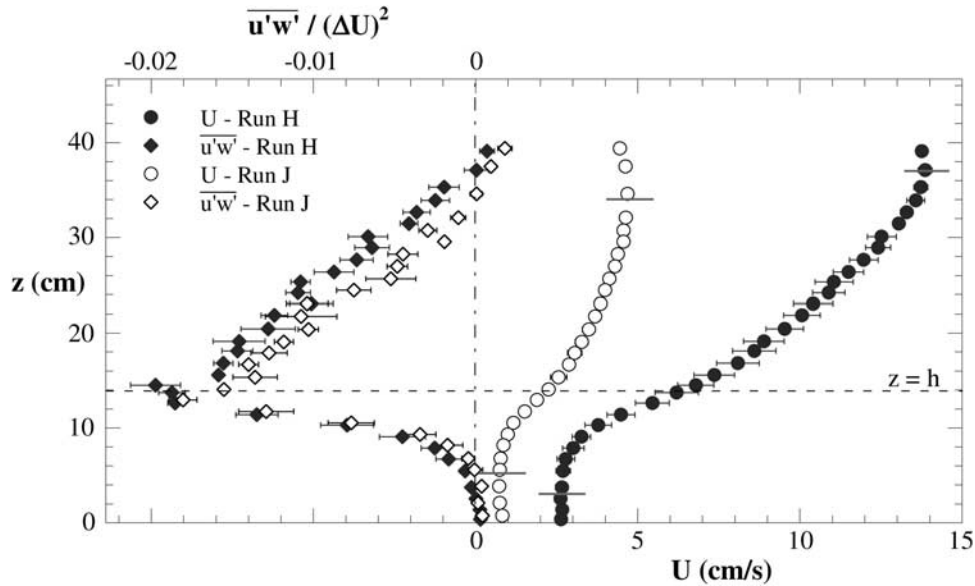


Figure 3. Vertical profiles of U and $\overline{u'w'}$ for run H ($S = 1.0 \times 10^{-4}$) and run J ($S = 1.3 \times 10^{-5}$). An increase in surface slope causes a slight increase in shear layer thickness and penetration. The value of $|\overline{u'w'}|$ is approximately $0.02(\Delta U)^2$ at the top of the canopy and decreases linearly above the canopy to a value of zero at $z \approx z_2$. The thick horizontal lines indicate the limits of the shear layers. The thin horizontal bars represent the standard uncertainties in the lateral means of U and $\overline{u'w'}$. In some instances, this measure is smaller than the marker.

Figure 3. Below the mixing layer ($z < z_1$), the Reynolds stress and velocity shear are both negligible. The value of $|\overline{u'w'}|$ increases upward through the canopy to approximately $0.02(\Delta U)^2$ at the canopy top and then decreases linearly above the canopy to a value of zero at $z \approx z_2$. The maximum shear occurs not at the drag discontinuity but at an average of 1.2 cm ($\approx 2d$) below the top of the canopy. This is due presumably to a greatly reduced drag coefficient near the free end of the cylinders, as will be shown in section 4.3. The Reynolds stress, however, is maximized exactly at the top of the canopy, providing the first indication of a reduction in the rate of vertical turbulent transport within the canopy. Figure 3 highlights the following trend shown in Table 1. For a given value of a (0.08 cm^{-1} in Figure 3), increasing the surface slope ($S = 1.3 \times 10^{-5}$ and 1.0×10^{-4} for runs J and H, respectively) increases the shear layer thickness (t_m) and the shear layer penetration into the canopy ($h - z_1$). This is due predominantly to the reduction in drag coefficient with increasing cylinder Reynolds number. Table 1 also shows an inverse correlation ($r^2 = 0.8$) between a (the packing density) and α (the fraction of the shear layer within the canopy). That is, denser arrays act as a stronger sink of vortex energy and thus allow less vortex penetration therein.

[16] A distinct correlation was observed between the normalized shear ($\Delta U/U_h$) and the dimensionless plant density (ad) (Figure 4), namely,

$$\frac{\Delta U}{U_h} \approx 16(ad) + 1, \quad 0.016 < ad < 0.081. \quad (11)$$

While it is not surprising that denser arrays generate more shear, we would expect that $\Delta U/U_h$ would also be proportional to C_D . However, the data in this study do not

bear out a dependence upon the drag coefficient; considering the $ad = 0.051$ data, the observed values of $\Delta U/U_h$ vary by only 4%, despite a 35% variation in a representative drag coefficient, C_{Dh} , defined in section 4.4 and listed in Table 1. It is important to note that equation (11) is only valid within the experimental range $0.016 < ad < 0.081$. We currently

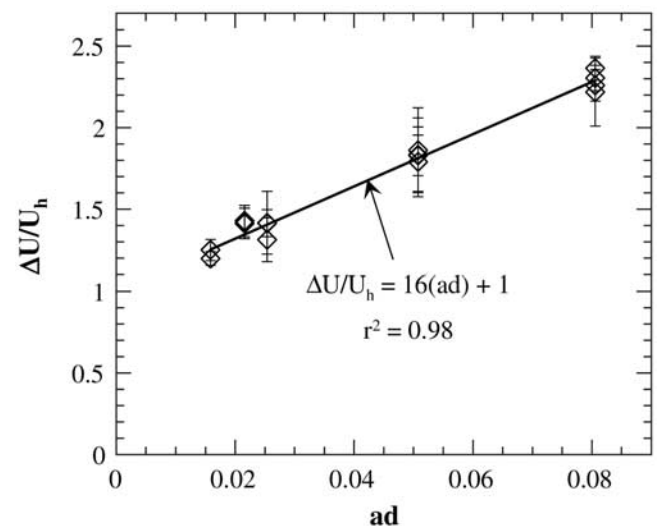


Figure 4. The correlation between the normalized shear ($\Delta U/U_h$) and the dimensionless plant density (ad). The $ad = 0.081$ data come from experiments in which the shear layers penetrated to the bed ($d = 0.64 \text{ cm}$, $h = 7.1 \text{ cm}$, provided by M. Ghisalberti (unpublished data, 2002)). The vertical bars represent the standard uncertainty in the lateral mean of $\Delta U/U_h$.

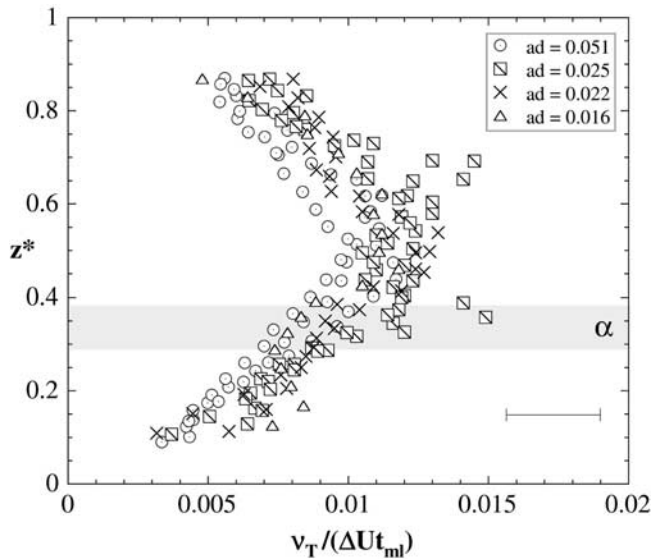


Figure 5. Vertical profiles of eddy viscosity (ν_T) throughout the shear layers. The data have been normalized by $\Delta U t_{ml}$ and are grouped according to their value of ad . The vertical scale, z^* , represents the distance from the bottom of the shear layer (z_1) normalized by the shear layer thickness (t_{ml}). The shaded area represents the range of locations of the canopy top ($z^* = \alpha$). The collapse of the profiles of $\nu_T / \Delta U t_{ml}$ is excellent, validating the assumption of a universal form of $f(z^*)$ in vegetated shear layers. The horizontal bar is representative of the standard uncertainty in each data point.

have insufficient data from sparse canopies to speculate on the behavior of the curve below $ad = 0.016$. In extremely sparse canopies where the canopy contribution to drag is much less than the bed contribution, the mixing layer analogy will break down completely and the scaling in Figure 4 will be invalid.

[17] As shown in Figure 3, the flow above the shear layer cannot be described by the one-dimensional momentum balance in equation (1). This is likely the result of secondary currents. As described by Ghisalberti and Nepf [2002], the shear layer vortices have a finite width ($b_v \approx t_{ml}/2$) and the flow is divided laterally into several subchannels of this width. Each subchannel contains a vortex street that is out of phase with those in neighboring subchannels. It is expected that cellular secondary currents develop within each subchannel, much as secondary currents are generated between neighboring longitudinal bed forms in rivers [see Nezu and Nakagawa, 1993]. We suggest that these secondary currents are not generated by the flume walls, but rather are inherent to flows with submerged vegetation. This assertion is supported by the fact that vegetated shear layers generated in a wide flume ($2.3 < b/H < 5.5$) [Dunn et al., 1996] exhibit the same growth behavior as the shear layers in this study ($b/H = 0.8$) [see White et al., 2003].

4.2. Vertical Profiles of Eddy Viscosity and Mixing Length

[18] This section examines the vertical profiles of eddy viscosity (ν_T) and specifically the validity of the critical assumption that $f(z^*)$ ($= \nu_T(z^*) / C_1 \Delta U t_{ml}$, from equation (5)) has a universal form in vegetated shear layers. First, point estimates of $\partial U / \partial z$ were obtained using central differencing.

Then the vertical profiles of both $\partial U / \partial z$ and $\overline{u'w'}$ were smoothed using a weighted, five-point moving average. The smoothed values of $\partial U / \partial z$ and $\overline{u'w'}$ were used in equation (5) to estimate ν_T . With the data grouped according to their value of ad , Figure 5 depicts the profiles of eddy viscosity (normalized by $\Delta U t_{ml}$) in the shear layers. Note that the vertical scale in this figure is z^* , the distance from the bottom of the shear layer (z_1) normalized by the shear layer thickness (t_{ml}). Because of the differencing and smoothing processes, only values within the range $0.1 \leq z^* \leq 0.9$ could be determined. The data from runs B and K were not included in this analysis because the measured values of $|\overline{u'w'}|$ within the shear layer ($O(10^{-2} \text{ cm}^2 \text{ s}^{-2})$) were not significantly greater than the noise levels of the ADV probes ($O(10^{-2} \text{ cm}^2 \text{ s}^{-2})$) [Voulgaris and Trowbridge, 1998]. The collapse of the profiles of ν_T (normalized by $\Delta U t_{ml}$) is excellent, validating the assumption of a singular form of $f(z^*)$ in vegetated shear layers. As expected, the eddy viscosity takes a maximum value (of roughly $0.012 \Delta U t_{ml}$) in the center of the shear layer ($z^* = 0.5$), irrespective of α .

[19] The validity of a constant mixing length model was also examined, as this will be used in section 5 to predict the velocity profile. The vertical mixing length l is defined by

$$l^2 = \frac{-\overline{u'w'}}{(\partial U / \partial z)^2} \quad (12)$$

and would be expected to scale upon t_{ml} . Figure 6 depicts the vertical profiles of l / t_{ml} . The assumption of a constant

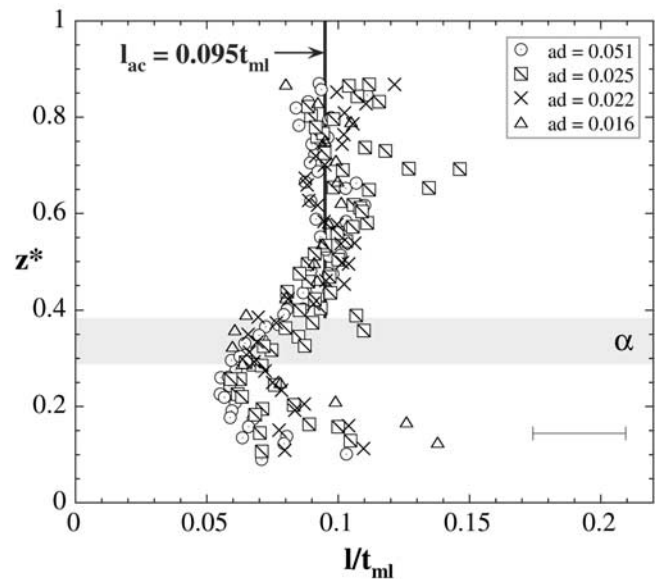


Figure 6. Vertical profiles of mixing length (l) throughout the shear layers. The data have been normalized by t_{ml} and are grouped according to their value of ad . The vertical scale is as in Figure 6. The shaded area represents the range of locations of the canopy top ($z^* = \alpha$). The mixing length varies little throughout the shear layer; the standard deviation of all values is less than 20% of the mean. For modeling purposes, the mean mixing length above the canopy (l_{ac}) is $0.095 t_{ml}$. The horizontal bar is representative of the standard uncertainty in each data point.

mixing length throughout the shear layer is quite reasonable as the standard deviation of all values is less than 20% of the mean. In the upper half of the mixing layer, the mixing length is constant ($(0.10 \pm 0.01) t_{mi}$) and the collapse of the data is excellent. Below this region, there is a smooth transition to a minimum value just below the canopy top (located at $z^* = \alpha$). It is worth noting that similarly depressed values are observed near the top of canopies that are more dense ($ad = 0.081$, provided by M. Ghisalberti (unpublished data, 2002)) and less dense ($ad = 0.007$, from Lopez and Garcia [1997]) than those employed in this study. For modeling purposes, the mean mixing length above the canopy (l_{ac}) is $0.095 t_{mi}$.

[20] Moving downward into the canopy, l increases and takes significantly larger values in the sparser arrays. It was initially thought that the profile of l within the canopy arose from the vertical variation in C_D (as will be discussed in section 4.3). However, even with C_D assumed constant in a k - ε model, Lopez and Garcia [1997] predicted that l reaches a local maximum within the canopy and then tends toward zero at the bottom of the shear layer. Examination of the unsmoothed statistics of this study, as well as experiments in which the shear layers penetrated to the bed ($h = 7.1$ cm, $ad = 0.081$, provided by M. Ghisalberti (unpublished data, 2002)), reveals that all vertical profiles of l (with the exception of run J) do indeed exhibit local maxima deep within the canopy. That the maxima occur at a fairly consistent distance ($0.10 \pm 0.03 t_{mi}$) from z_1 , and not the bed (1–8 cm), suggests that boundary effects are not responsible. Finally, the values of l at the limits of the shear layer make physical sense. At z_1 , all vortical motion has been dissipated by the canopy elements, so l should approach zero. Above the canopy there is no drag dissipation, so l is expected to maintain its constant value to z_2 , as demonstrated by the unsmoothed data and by Lopez and Garcia [1997].

[21] For modeling purposes, the slight vertical variation of l within the canopy will be ignored. The mean in-canopy mixing length (l_c) for each run was taken as the average of the unsmoothed values, where a linear extrapolation from the local maximum to zero at $z = z_1$ was applied. The mean normalized in-canopy mixing length (l_c/t_{mi}) correlates well with the penetration ratio (α). Considering all nine runs in Figure 6,

$$\frac{l_c/t_{mi}}{\alpha} = 0.22 \pm 0.01. \quad (13)$$

This indicates that the destruction of vortical motion by the canopy decreases the in-canopy mixing length and the extent of vortex penetration to the same degree. In an infinitely sparse array (for which we would expect $\alpha = 0.5$), the mean mixing length based on equation (13) approaches the value observed well above the canopy ($0.1 t_{mi}$), as expected.

[22] An approximately constant mixing length in vegetated aquatic shear layers contrasts sharply with the terrestrial analogue, in which vertical turbulent length scales increase with height [see, e.g., Raupach *et al.*, 1996]. Terrestrial vegetated shear layers are, however, embedded within an atmospheric boundary layer of a much larger scale. The height-dependence of vertical length scales is

indicative of the extent to which boundary-layer-scale turbulence affects transport within terrestrial vegetated shear layers. In aquatic flows, the general absence of an extensive overlying boundary layer should allow an approximately constant mixing length (that scales upon the vortex size) throughout the shear layer, irrespective of the canopy density.

4.3. Drag Coefficient of a Submerged Array

[23] While characterization of the drag coefficient (C_D) for arrays of submerged cylinders was not a focus of this study, it is a necessary step toward evaluating Ω (equation (9)) and modeling the flow. As a framework, we first consider established relationships for the drag coefficient from previous studies. The drag coefficient of an isolated, infinite, smooth cylinder (C_{DC}) is well known, its dependence on Reynolds number (Re_d) having the form

$$C_{DC} \approx 1.0 + 10.0(Re_d)^{-2/3}, \quad 1 < Re_d < 2 \times 10^5 \quad (14)$$

[White, 1974, p. 210].

[24] For an array of submerged cylinders, however, wake interactions and finite cylinder length will both affect the drag coefficient (C_D). Unfortunately, these effects have not been comprehensively evaluated. The turbulence of upstream wakes delays separation on downstream cylinders, resulting in a lower drag [Zukauskas, 1987]. Although the transition to a turbulent wake structure within a sparse ($ad < 0.1$), emergent array is expected to occur at $Re_d \geq 200$ [Nepf, 1999], the shear-layer-scale turbulence sweeping through submerged arrays may trigger wake turbulence at lower local Reynolds numbers. Bokaian and Geoola [1984] quantitatively described the suppression of the drag coefficient of a cylinder when in the wake of an upstream cylinder and its dependence upon the relative positions of the two cylinders. Using this information, Nepf [1999] conducted a numerical experiment to evaluate the bulk drag coefficient of an emergent array by assuming that the reduction in the drag coefficient of an individual cylinder is due entirely to the wake of the nearest upstream cylinder. The author found that the bulk drag coefficient (C_{DA}) of a random, emergent array of cylinders at high Reynolds number decreases with increasing cylinder density (ad), according to the best fit polynomial

$$C_{DA} = \frac{C_{DC}}{1.16} \left\{ 1.16 - 9.31(ad) + 38.6(ad)^2 - 59.8(ad)^3 \right\} \quad (15)$$

for $ad < 0.1$. The agreement between experimental data from random, emergent arrays with $Re_d > 200$ and the expression in equation (15) is very good [Nepf, 1999].

[25] The free end of a cantilevered circular cylinder generates strong longitudinal vortices near the tip that cause considerable disturbance to the wake structure. The effect of this free-end disturbance is to increase the wake pressure, leading to a reduction in drag, as compared with an infinitely long cylinder. For a single cylinder with a large aspect ratio ($h/d > 13$) at high Reynolds number ($Re_d \approx 4 \times 10^4$), the magnitude of drag coefficient suppression is independent of aspect ratio and is confined to a region that extends $20d$ from the free end [Fox and West, 1993]. In such cases, the minimum drag coefficient is roughly $0.7 C_{DC}$.

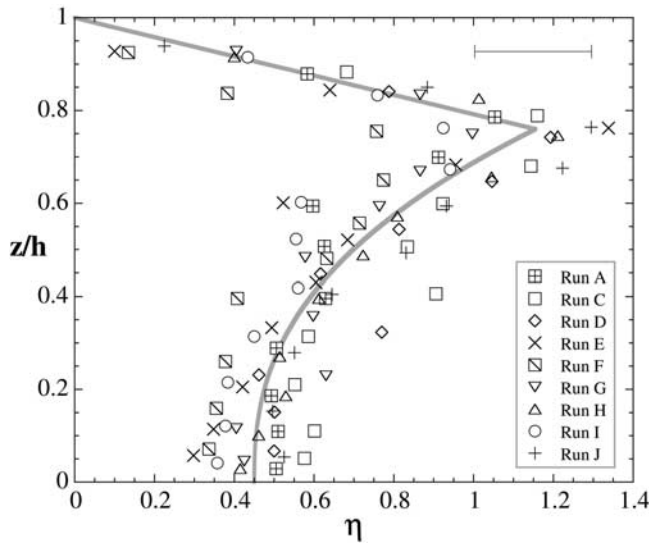


Figure 7. Vertical profiles of η , the ratio of the observed drag coefficient to the theoretical value predicted by considering array density and Reynolds number effects. The solid line is a best fit curve through all points, and has the form shown in equation (18). The horizontal bar is representative of the standard uncertainty in each data point.

[26] The data of *Luo et al.* [1996] show that a submerged cylinder ($h/d = 8$) placed a distance $5d$ immediately behind another submerged cylinder has a mean drag coefficient roughly equal to that predicted by combining upstream proximity and free-end effects. However, shear-scale turbulence in the free stream of vegetated shear flows will undoubtedly alter these effects and the interaction between them. Because no previous studies enable accurate prediction of $C_D(z)$, an empirical form was sought in these experiments for subsequent use in the numerical model.

[27] For each experimental run, the vertical profile of the drag coefficient within the canopy was evaluated using equation (1), i.e.,

$$C_D(z) = \frac{2(gS - \partial(\overline{u'w'})/\partial z)}{aU^2(z)}. \quad (16)$$

The vertical gradient of $\overline{u'w'}$ was evaluated using a central difference. The ratio of the observed drag coefficient to that for an infinite cylinder array (C_{DA} , evaluated using the depth-specific velocity) will be defined as

$$\eta(z) = \frac{C_D(z)}{C_{DA}(z)}. \quad (17)$$

This parameter explicitly describes the effects of the free end on the drag coefficient of the array. The vertical profiles of η for the experimental arrays are shown in Figure 7. As in section 4.2, runs B and K were not included in this analysis because of uncertainty in recorded values of $\overline{u'w'}$. The collapse of η is good across all flow conditions, with no discernible dependence upon Re_d or ad . From a value of roughly 0.45 at the bed, η increases toward the free end, taking a maximum value of approximately 1.2 at $z/h \approx 0.76$. Above this point, η decreases steadily to zero at the top of

the cylinders. The collapsed profiles of η are in fair qualitative agreement with the data of *Dunn et al.* [1996] ($ad = 0.002 - 0.016$). The best fit curve shown in Figure 7 takes the form

$$\eta = \begin{cases} 1.4\left(\frac{z}{h}\right)^{2.5} + 0.45, & 0 \leq z/h \leq 0.76 \\ -4.8\left(\frac{z}{h}\right) + 4.8, & 0.76 < z/h \leq 1 \end{cases}. \quad (18)$$

4.4. Behavior of the Stability Parameter

[28] To facilitate evaluation of the stability parameter (Ω), the product $C_{Dh}\overline{\eta}$ was chosen as a representative bulk drag coefficient for the submerged arrays. C_{Dh} is the value of C_{DA} at the top of the canopy (see Table 1) and accounts for the effects of Reynolds number and packing density on the drag coefficient. The parameter $\overline{\eta}$ represents the arithmetic average of $\eta(z)$ within the shear layer and accounts for free-end effects. Since $z_1/h < 0.76$ for all runs, from equation (18),

$$\begin{aligned} \overline{\eta} &= \frac{1}{1-\beta} \int_{\beta}^1 \eta(z/h) d(z/h) \\ \overline{\eta} &= \frac{0.63 - 0.4\beta^{3.5} - 0.45\beta}{1-\beta}, \end{aligned} \quad (19)$$

where $\beta = z_1/h$.

[29] The estimated values of Ω (8.7 ± 0.5), evaluated using equation (9) and $C_D = C_{Dh}\overline{\eta}$, are remarkably constant (Figure 8). Furthermore, Ω exhibits no dependence upon α , suggesting that this constancy extends beyond the experimental range of $0.29 < \alpha < 0.38$. The universal constancy of Ω validates the analysis presented in section 2 and confirms that the growth of vegetated shear layers ceases once the production and dissipation of SKE are equal.

[30] Interestingly, Ω is independent of both Reynolds numbers that characterize vegetated shear flows: that of the individual cylinders ($Re_d = U_h d/\nu$) and that of the mixing layer ($Re_{ml} = \Delta U t_{ml}/\nu$). Specifically, Ω is independent of whether Re_{ml} is less than, within, or greater than the observed range for transition in mixing layers ($\approx 6 \times 10^3$ to 2×10^4). This is not unexpected, as the transition has a strong effect on small-scale scalar mixing but not on shear layer growth [*Moser and Rogers, 1991*]. Also note that in several runs, $Re_d < 200$ (Table 1), violating a requirement of using equation (15) to predict C_D [*Nepf, 1999*]. However, the values of Ω exhibit little dependence on Re_d , and the use of equation (15) in this context appears appropriate for $Re_d \geq 60$.

5. Numerical Model of Vegetated Shear Flow

[31] Having identified the stability constant (Ω) and a mixing length model for Reynolds stress closure, we now use these universal functions to predict the vertical velocity profile of vegetated shear flows. A one-dimensional numerical model of equation (1) was created to determine if experimental velocity profiles could be accurately predicted under the assumptions of constant Ω and mixing length (l_{ac} above the canopy and l_c within). The model requires as input the canopy parameters a , d , and h , the slope S , and the form of $\eta(z)$.

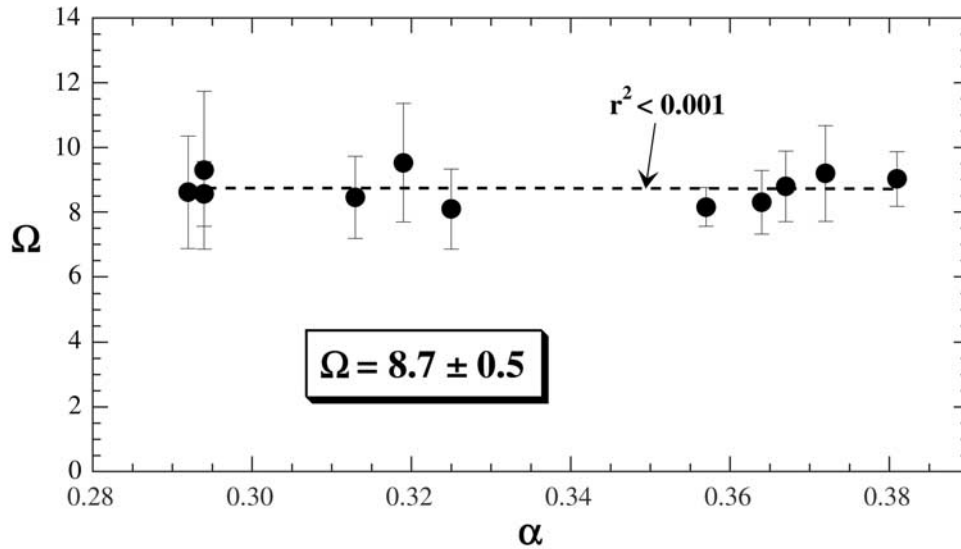


Figure 8. The invariability of the stability parameter Ω . The standard deviation (0.5) of the observed values of Ω around the mean (8.7) is very small. There is no dependence of Ω on α , as indicated by the dashed line of regression. The constancy of Ω confirms that shear layer growth ceases once the production and dissipation of SKE are equal. The vertical bars represent the standard uncertainty in the lateral mean of Ω .

[32] In the model, the flow was divided into two regions: the portion of the shear layer within the canopy (i.e., $z_1 \leq z \leq h$, zone 1) and the portion of the shear layer above the canopy (i.e., $h < z \leq z_2$, zone 2). Below z_1 , the velocity is assumed to be independent of depth and dictated solely by a balance of pressure and drag forces. The nature of the velocity profile above the shear layer was not explored here and will certainly depend upon the fraction of the depth that the region encompasses ($1 - (z_2/H)$). The model assumes a constant mixing length (l_c) within zone 1, such that equation (1) becomes

$$\frac{\partial}{\partial z} \left[\left(\frac{\partial U}{\partial z} \right)^2 \right] = \frac{1}{l_c^2} \left(\frac{1}{2} C_D a U^2 - gS \right) \quad [\text{zone 1}], \quad (20)$$

which must be solved numerically. However, an analytical solution can be found in zone 2. With a constant mixing length, $l_{ac} = 0.095 t_{ml}$, and an absence of drag, equation (1) becomes

$$\frac{\partial}{\partial z} \left[\left(\frac{\partial U}{\partial z} \right)^2 \right] = \frac{-gS}{(0.095 t_{ml})^2}, \quad (21)$$

Table 2. Summary of Modeling Equations for the i th Point in Zone 1

Parameter	Modeling Equation
Velocity profile	1. $\left(\frac{\partial U}{\partial z} \right)_i^2 = \left(\frac{\partial U}{\partial z} \right)_{i-1}^2 + \left[\frac{1}{l_c^2} \left(\frac{1}{2} C_{D,i-0.5} a U_{i-0.5}^2 - gS \right) \right] \Delta z$ 2. $U_i = U_{i-1} + \left(\frac{\partial U}{\partial z} \right)_{i-0.5} \Delta z$
Drag coefficient	$C_{D,i} = \eta_i C_{DA,i}$ ^a
Mixing length	$l_c = 0.22(h - z_1)$, from equation (13)

^aThe function $\eta(z/h)$ is given in equation (18), and $C_{DA}(z)$ is given in equation (15).

which has the solution

$$U(z) = U_h + \frac{2\sqrt{gS}}{3(0.095 t_{ml})} \left\{ (z_2 - h)^{3/2} - (z_2 - z)^{3/2} \right\} \quad [\text{zone 2}]. \quad (22)$$

[33] The equations that form the basis of the numerical model of zone 1 are shown in Table 2, where $\Delta z (= (h - z_1)/400)$ is the chosen distance between grid points. The subscript i specifies the grid point number. The use of $i - 0.5$ indicates that the value taken is the mean of values at points i and $i - 1$. The first equation in the table is a discretization of equation (20). As U , $\partial U/\partial z$, and C_D are all interdependent, the model was created in Microsoft Excel, which iterates the modeling equations to determine the solution ($U_i(z)$). The results of a model based on equations (20) and (22) will depend heavily upon where the model is initiated (z_1) and where the shear layer ends (z_2). We thus require two independent relationships that permit the evaluation of these end points. The first relationship is obtained from the definition of the stability parameter in equation (9), with $\Omega = 8.7$ and $C_D = C_{Dh}\bar{\eta}$ as described above:

$$h - z_1 = \frac{1}{8.7 C_{Dh} \bar{\eta} a} \left(\frac{(\Delta U)^2}{U_h^2 - U_1^2} \right). \quad (23)$$

To avoid the interdependence of all variables, it was also necessary to utilize a relationship between characteristics of the shear layer and of the vegetation. To this end, the dependence of the normalized shear ($\Delta U/U_h$) on solely the dimensionless plant density (ad) (shown in equation (11)) was also employed.

[34] The model is initiated at the base of the shear layer (z_1), where $U = U_1$ and $\partial U/\partial z = 0$. Under the assumption of zero Reynolds stress below the shear layer, U_1 is predicted

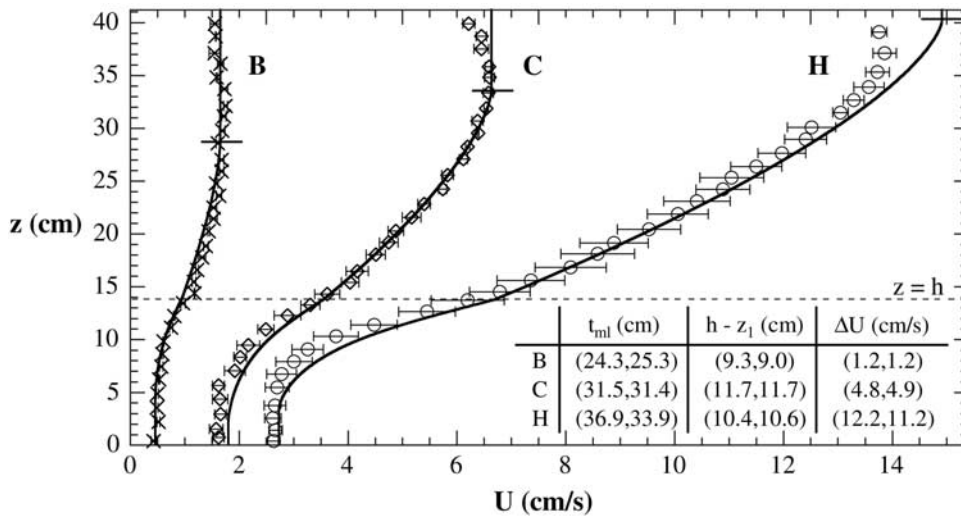


Figure 9. A comparison between observed (marker) and predicted (solid line) profiles of mean velocity for runs B ($a = 2.5 \text{ m}^{-1}$), C (3.4 m^{-1}), and H (8 m^{-1}). The thin horizontal bars represent the lateral variability of the observed velocity. The thick horizontal lines indicate the predicted values of z_2 ; the model is not strictly valid above this point. The table compares the predicted and observed values (P,O) of t_{ml} , $h - z_1$ and ΔU . Over all runs, the model predicts the values of each of these three parameters to within an average of 7%.

from a balance of pressure and drag forces in equation (1) (i.e., $U_1 = \sqrt{2gS/C_D(z_1)a}$). As $C_D(z_1)$ ($= \eta(z_1)C_{DA}(z_1)$) is itself a function of U_1 , a simple iteration is required. The most accurate predictions of U_1 were obtained with $\eta(z_1) = 0.38$, which lies within the range of values observed deep within the canopy (0.45 ± 0.15) in Figure 7. The model then requires the following iteration:

[35] 1. First, initial guesses of z_1 and t_{ml} are made. On the basis of results of this study, good initial values are $z_1 \approx h - 0.4a^{-1}$ and $t_{ml} \approx (h - z_1)/0.33$.

[36] 2. Then, with the initial conditions of $(U, \partial U/\partial z)_{z_1} = (U_1, 0)$, the equations described in Table 2 are used to evaluate $U(z)$ up to $z = h$.

[37] 3. With the value of U_h obtained in step 2, and the guessed values of z_1 and t_{ml} from step 1, the velocity profile above the canopy (up to $z = z_2 = z_1 + t_{ml}$) is determined using equation (22).

[38] 4. From the complete profile, the value of $\Delta U/U_h$ is evaluated. The value of t_{ml} is then varied, and steps 2–4 are repeated, until $\Delta U/U_h$ takes the value required by equation (11).

[39] 5. On the basis of the stability analysis, the required value of z_1 is calculated using equation (23). If the required value does not agree with the initial guess, we return to step 1 and take the required value as the next guess. Steps 1–5 are repeated until the required value of z_1 agrees with the guessed value. The final velocity profile then satisfies both conservation of momentum and the criterion defined by the stability parameter.

5.1. Comparison Between the Model and Experimental Data

[40] The agreement between the observed velocity profiles and those predicted by the model is very good, as shown in Figure 9. The predicted values of t_{ml} , $h - z_1$, and ΔU all deviated from observed values by, on average, less than 7%. As a constant in-canopy mixing length was

employed, the curvature of the velocity profile within the canopy cannot be modeled exactly. In addition, the velocity gradient has a discontinuity at $z = h$ because of the assumed discontinuity in mixing length. Note that the model is only used to predict $U(z)$ within the region $0 < z < z_2$. Above z_2 , the velocity begins to decrease as $\overline{u'w'}$ becomes positive (Figure 3). The exact nature of the velocity profile above this point could not be determined with the ADV and was not modeled. Finally, there is excellent agreement between the predicted and observed values of ΔU over a wide range of that parameter, as

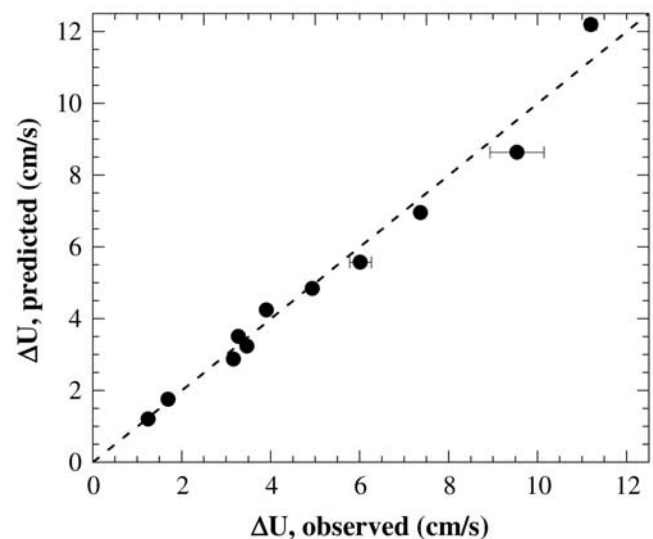


Figure 10. The comparison between observed values of ΔU and those predicted by the model. The dashed line indicates perfect agreement. The horizontal bars represent the lateral variability in the observed value of ΔU .

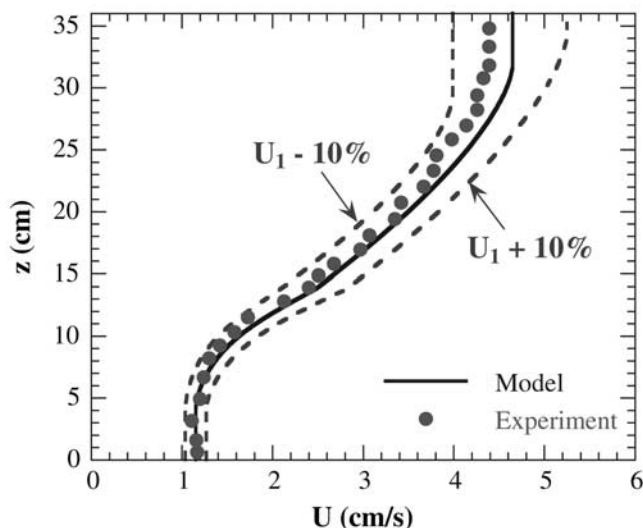


Figure 11. Demonstration of model sensitivity to the chosen value of U_1 . The figure shows the model prediction for run G, using three values of U_1 : (1) the value predicted using $\eta(z_1) = 0.38$ (1.15 cm/s), (2) a value 10% greater than that predicted (1.27 cm/s), and (3) a value 10% less than that predicted (1.04 cm/s). The model predictions of t_{ml} and ΔU are sensitive to a 10% variation in U_1 , changing by roughly 9% and 15%, respectively. The predicted value of shear layer penetration into the canopy, $h - z_1$, is much less sensitive, changing by only 1%.

demonstrated in Figure 10. Note that while $\Delta U/U_h$ is prescribed by equation (11), U_h is predicted independently, so the accuracy of predicted ΔU values is an independent check of model performance. The good agreement shown in Figure 10 indicates that the model is accurate across the gamut of experimental conditions.

[41] The sensitivity of the model to changes in the value of U_1 is highlighted by Figure 11, which demonstrates how predicted velocity profiles for run G vary with U_1 . The predicted values of t_{ml} and ΔU are quite sensitive to a 10% variation in U_1 , changing by roughly 9% and 15%, respectively. The predicted value of $h - z_1$ is relatively insensitive, changing by less than 1%. That the accuracy of the model relies heavily upon the accurate prediction of U_1 reinforces the importance of quantifying the drag coefficients of submerged canopies.

5.2. Extension of the Model to Field Conditions

[42] First, it is important to note that the analysis described in this paper applies only to completely unbounded vegetated shear layers, i.e., shear layers that extend neither to the free surface nor to the bed. The agreement between model and experiment demonstrates that assumptions of constant mixing lengths (l_c , l_{ac}) and a universal stability parameter (Ω) lend themselves to accurate predictions of the velocity profile within and above dense aquatic canopies. However, to extend the model to the field, several pieces of information are required. For example, the relationship between $\Delta U/U_h$ and ad in sparse canopies ($ad < 0.016$) must be ascertained. Potentially the biggest obstacle to field application of the model, however, is the lack of knowledge concerning $C_D(z)$. The profile

used in this study, described by equations (18) and (15), is strictly valid only for cylinders with $h/d \approx 22$ within the experimental range of $130 < Re_d < 460$. Further research into the dependence of $C_D(z)$ upon the aspect ratio, packing density, Reynolds number, and morphology of submerged canopies is much needed. In the limit of infinitely thin vegetation ($h/d \rightarrow \infty$), however, the assumption of a constant C_D (evaluated using equation (15)) may be appropriate. Furthermore, the experiments in this study used rigid dowels to simulate submerged, aquatic vegetation. In reality, such vegetation is often flexible and can exhibit pronounced coherent waving (monami) in a unidirectional current [Ackerman and Okubo, 1993; Grizzle et al., 1996]. The monami can significantly increase the penetration of turbulent stress into the canopy, as the waving reduces the drag exerted by the vegetation [Ghisalberti and Nepf, 2002]. A means of estimating temporal averages of $(C_D a)$ is therefore required before application of this model to waving canopies.

6. Conclusion

[43] It was postulated that the growth of vegetated shear layers ceases once the production of shear-layer-scale turbulent kinetic energy is balanced by drag dissipation. This was confirmed by flume experiments, which showed that a scaled ratio of production to dissipation is a constant ($\Omega = 8.7 \pm 0.5$) for fully developed vegetated shear layers. This stability constant was used to close a one-dimensional numerical model that predicts the vertical velocity profile of vegetated shear flows. The model also uses the assumption of a single mixing length above the vegetation and a single, reduced mixing length within it. The agreement between model and experiment is good, but field application of the model is limited by a lack of description of the drag coefficient in real canopies.

[44] **Acknowledgments.** This material is based upon work supported by the National Science Foundation under grant 0125056. Any opinions, findings, and conclusions or recommendations expressed in this material are those of the authors and do not necessarily reflect the views of the National Science Foundation.

References

- Ackerman, J. D., and A. Okubo (1993), Reduced mixing in a marine macrophyte canopy, *Funct. Ecol.*, 7, 305–309.
- Bokaian, A., and F. Geoola (1984), Wake-induced galloping of two interfering circular cylinders, *J. Fluid Mech.*, 146, 383–415.
- Brown, G. L., and A. Roshko (1974), On density effects and large structure in turbulent mixing layers, *J. Fluid Mech.*, 64, 775–816.
- Brunet, Y., J. J. Finnigan, and M. R. Raupach (1994), A wind tunnel study of air flow in waving wheat: Single-point velocity statistics, *Boundary Layer Meteorol.*, 70, 95–132.
- Burke, R. W., and K. D. Stolzenbach (1983), Free surface flow through salt marsh grass, *MIT Sea Grant Tech. Rep.*, 83-16, Mass. Inst. of Technol., Cambridge, Mass.
- Butman, C. A. (1987), Larval settlement of soft-sediment invertebrates: The spatial scales of pattern explained by active habitat selection and the emerging role of hydrodynamical processes, *Oceanogr. Mar. Biol.*, 25, 113–165.
- Chandler, M., P. Colarusso, and R. Buschsbaum (1996), A study of eelgrass beds in Boston Harbor and northern Massachusetts bays, report, U.S. Environ. Prot. Agency, Narragansett, R. I.
- Chu, V. H., and S. Babarutsi (1988), Confinement and bed-friction effects in shallow turbulent mixing layers, *J. Hydraul. Eng.*, 114(10), 1257–1274.
- Corrsin, S. (1974), Limitations of gradient transport models in random walks and in turbulence, *Adv. Geophys.*, 18A, 25–60.

- Duggins, D., J. Eckman, and A. Sewell (1990), Ecology of understory kelp environments: II. Effects of kelps on recruitment of benthic invertebrates, *J. Exp. Mar. Biol. Ecol.*, *143*, 27–45.
- Dunn, C., F. Lopez, and M. Garcia (1996), Mean flow and turbulence in a laboratory channel with simulated vegetation, *Hydraul. Eng. Ser. 51, UIIU-ENG-96-2009*, Dep. of Civ. Eng., Univ. of Ill. at Urbana-Champaign, Urbana, Ill.
- Eckman, J. (1983), Hydrodynamic processes affecting benthic recruitment, *Limnol. Oceanogr.*, *28*, 241–257.
- Finnigan, J. (2000), Turbulence in plant canopies, *Annu. Rev. Fluid Mech.*, *32*, 519–571.
- Fox, T. A., and G. S. West (1993), Fluid-induced loading of cantilevered circular cylinders in a low-turbulence uniform flow: I. Mean loading with aspect ratios in the range 4 to 30, *J. Fluid. Struct.*, *7*, 1–14.
- Gambi, M. C., A. R. M. Nowell, and P. A. Jumars (1990), Flume observations on flow dynamics in *Zostera marina* (eelgrass) beds, *Mar. Ecol. Prog. Ser.*, *61*, 159–169.
- Ghisalberti, M., and H. M. Nepf (2002), Mixing layers and coherent structures in vegetated aquatic flows, *J. Geophys. Res.*, *107*(C2), 3011, doi:10.1029/2001JC000871.
- Grizzle, R., F. Short, C. Newell, H. Hoven, and L. Kindblom (1996), Hydrodynamically induced synchronous waving of seagrasses: “Monami” and its possible effects on larval mussel settlement, *J. Exp. Mar. Biol. Ecol.*, *206*(1–2), 165–177.
- Ikeda, S., and M. Kanazawa (1996), Three-dimensional organized vortices above flexible water plants, *J. Hydraul. Eng.*, *122*(11), 634–640.
- Koochesfahani, M. M., and P. E. Dimotakis (1986), Mixing and chemical reactions in a turbulent liquid mixing layer, *J. Fluid Mech.*, *170*, 83–112.
- Kouwen, N., and T. E. Unny (1973), Flexible roughness in open channels, *J. Hydraul. Div. Am. Soc. Civ. Eng.*, *99*(5), 713–728.
- Kouwen, N., T. E. Unny, and H. M. Hill (1969), Flow retardance in vegetated channels, *J. Irrig. Drain. Div. Am. Soc. Civ. Eng.*, *95*(2), 329–342.
- Lopez, F., and M. Garcia (1997), Open-channel flow through simulated vegetation: Turbulence modeling and sediment transport, *Wetlands Res. Program Rep. WRP-CP-10*, U.S. Army Corps of Eng., Washington, D. C.
- Lopez, F., and M. Garcia (2001), Mean flow and turbulence structure of open-channel flow through non-emergent vegetation, *J. Hydraul. Eng.*, *127*(5), 392–402.
- Luo, S. C., T. L. Gan, and Y. T. Chew (1996), Uniform flow past one (or two in tandem) finite length circular cylinder(s), *J. Wind. Eng. Ind. Aerodyn.*, *59*, 69–93.
- Moser, R. D., and M. M. Rogers (1991), Mixing transition and the cascade to small scales in a plane mixing layer, *Phys. Fluids A*, *3*(5), 1128–1134.
- Neary, V. S. (2003), Numerical solution of fully developed flow with vegetative resistance, *J. Eng. Mech.*, *129*(5), 558–563.
- Nepf, H. M. (1999), Drag, turbulence, and diffusion in flow through emergent vegetation, *Water Resour. Res.*, *35*(2), 479–489.
- Nepf, H. M., and E. R. Vivoni (2000), Flow structure in depth-limited, vegetated flow, *J. Geophys. Res.*, *105*(C12), 28,547–28,557.
- Nezu, I., and H. Nakagawa (1993), *Turbulence in Open-Channel Flows*, A. A. Balkema, Brookfield, Vt.
- Phillips, R. C., and E. G. Menez (1988), Seagrasses, *Smithson. Contrib. Mar. Sci.*, *34*, 1–104.
- Raupach, M. R., J. J. Finnigan, and Y. Brunet (1996), Coherent eddies and turbulence in vegetation canopies: The mixing-layer analogy, *Boundary Layer Meteorol.*, *78*, 351–382.
- Shaw, R. H., and I. Seginer (1985), The dissipation of turbulence in plant canopies, in *Proceedings of the 7th Symposium of the American Meteorological Society on Turbulence and Diffusion*, pp. 200–203, Am. Meteorol. Soc., Boston, Mass.
- Shi, Z., J. S. Pethick, and K. Pye (1995), Flow structure in and above the various heights of a saltmarsh canopy: A laboratory flume study, *J. Coast. Res.*, *11*, 1204–1209.
- Short, F. T., and C. A. Short (1984), The seagrass filter: Purification of estuarine and coastal waters, in *The Estuary as a Filter*, edited by V. S. Kennedy, pp. 395–413, Academic, San Diego, Calif.
- Short, F. T., W. C. Dennison, and D. G. Capone (1990), Phosphorus-limited growth of the tropical seagrass *Syringodium filiforme* in carbonate sediments, *Mar. Ecol. Prog. Ser.*, *62*, 169–174.
- Taylor, D., S. Nixon, S. Granger, and B. Buckley (1995), Nutrient limitation and the eutrophication of coastal lagoons, *Mar. Ecol. Prog. Ser.*, *127*, 235–244.
- Thom, A. S. (1971), Momentum absorption by vegetation, *Q. J. R. Meteorol. Soc.*, *97*, 414–428.
- Voulgaris, G., and J. H. Trowbridge (1998), Evaluation of the acoustic Doppler velocimeter (ADV) for turbulence measurements, *J. Atmos. Oceanic Technol.*, *15*, 272–289.
- White, B. L., M. Ghisalberti, and H. M. Nepf (2003), Shear layers in partially vegetated channels: Analogy to shallow water shear layers, paper presented at the International Symposium on Shallow Flows, Int. Assoc. for Hydraul. Eng. and Res., Delft Univ. of Technol., Delft, Netherlands, 16–18 June.
- White, F. M. (1974), *Viscous Fluid Flow*, McGraw-Hill, New York.
- Wilson, J. D. (1988), A second-order closure model for flow through vegetation, *Boundary Layer Meteorol.*, *42*, 371–392.
- Zhuang, Y., and B. D. Amiro (1994), Pressure fluctuations during coherent motions and their effects on the budgets of turbulent kinetic energy and momentum flux within a forest canopy, *J. Appl. Meteorol.*, *33*, 704–711.
- Zukauskas, A. (1987), Heat transfer from tubes in cross-flow, *Adv. Heat Transf.*, *18*, 87–159.

M. Ghisalberti and H. M. Nepf, Ralph M. Parsons Laboratory, Department of Civil and Environmental Engineering, Massachusetts Institute of Technology, 150 Albany Street, Cambridge, MA 02139, USA. (marcog@mit.edu; hmnepf@mit.edu)